

The Oceanic Variability Spectrum and Transport Trends

Carl Wunsch

Department of Earth, Atmospheric and Planetary Sciences

Massachusetts Institute of Technology

Cambridge MA 02139 USA

email: cwunsch@mit.edu

June 19, 2009

Abstract

Oceanic meridional transports evaluated over the width of the Pacific Ocean from altimetric observations become incoherent surprisingly rapidly with meridional separation. Even with 15 years of data, surface slopes show no significant coherence beyond 5° of latitude separation at any frequency. An analysis of the frequency/zonal-wavenumber spectral density shows a broad continuum of motions at all time and space scales, with a significant excess of energy along a “non-dispersive” line extending between the simple barotropic and first baroclinic mode Rossby waves. It is speculated that much of that excess energy lies with coupled barotropic and first mode Rossby waves. The statistical significance of apparent oceanic transport trends depends upon the existence of a reliable frequency/wavenumber spectrum and for which only a few observational elements now exist.

1 Introduction

A quantitative description of oceanic variability is useful for a number of reasons including the detection of climate trends, the testing of oceanic GCMs, and the identification and understanding of basic physical mechanisms in the ocean circulation. In particular, detection of supposed trends in the ocean circulation is now the subject of impressive expenditures (Schiermeier, 2004), and the interest of a large community worried about climate change (e.g., IPCC, 2007). A growing literature is accumulating around the goal of detecting oceanic trends, some of which is aimed at “early warning” of abrupt climate shifts. But the ocean is a very noisy place with variability on all time and space scales and with very long intrinsic memory (e.g., Peacock and Maltrud, 2006; Wunsch and Heimbach, 2008). Because of the long memory, most oceanographic time series display some form of apparent trend and the main issue is assigning a confidence

26 interval to the result to distinguish it from the random-walk behavior always present in long
27 time-scale systems (e.g., Percival et al., 2001). Determination of the significance of true trends
28 involves a deep understanding of the nature of oceanic variability generally. (Here, a “true
29 trend” is defined as one that would persist for several multiples of the data duration.) The goal
30 of understanding the apparent fluctuations in meridional volume transports as determined from
31 sea level variations is used to motivate a discussion of the nature of altimetric data sets. Trends
32 in sea level variations are of intense interest in their own right, but are not directly pursued here
33 (but see Wunsch et al., 2007 for discussion and references).

34 **2 Altimetric Velocities and Transports**

35 The longest observed time series available with near-global coverage are the high accuracy al-
36 timetry records that became available with the TOPEX-POSEIDON satellite beginning at the
37 end of 1992, providing (at the time of writing) about 15 years of usable data. We here briefly
38 describe the way in which altimetric data can be used to make some inferences about transport
39 variability and their link to the problem of trend determination. In practice, one seeks (Wunsch
40 and Heimbach, 2009) to combine the altimetric data with *all* available oceanographic data, but
41 the domination of the calculations by the volume of satellite data suggests the utility of the
42 present focus.

43 The major issue, and the one that provides the theme for what follows later, is that altimetry
44 produces estimates of the sea surface slope and hence of the surface geostrophic flow (to a high
45 degree of approximation) and discussions of climate variables require inferences about the entire
46 water column. Altimetry is only readily interpreted in volume (or mass) transport terms to the
47 extent that the surface geostrophic flow is primarily controlled by, or controls, a known vertical
48 structure. To interpret the results here, the approximation in Wunsch (1997) will be employed:
49 that the *surface* kinetic energy is dominantly that of the first baroclinic mode. The expression
50 “transport” is then used as a short-hand for the approximate volume transport in the first
51 baroclinic mode *above* above some arbitrary depth, possibly its zero crossing near 1000m as used
52 in Wunsch (2008). The reader is strongly cautioned, however, that as depicted in Wunsch (1997),
53 and as discussed below, water column variability is dominated in many, if not most, places
54 by the *barotropic* flow—and which is sometimes wholly omitted from theoretical discussions.
55 Here the terminology “barotropic” is used to denote the projection onto a vertically constant
56 horizontal velocity as determined e.g., from a flat-bottom linear dynamics ocean. Lapeyre and
57 Klein (2006), have shown that there can exist near-surface trapped balanced motions owing
58 to a finite buoyancy flux through the sea surface. In the linear limit, these are the trapped,

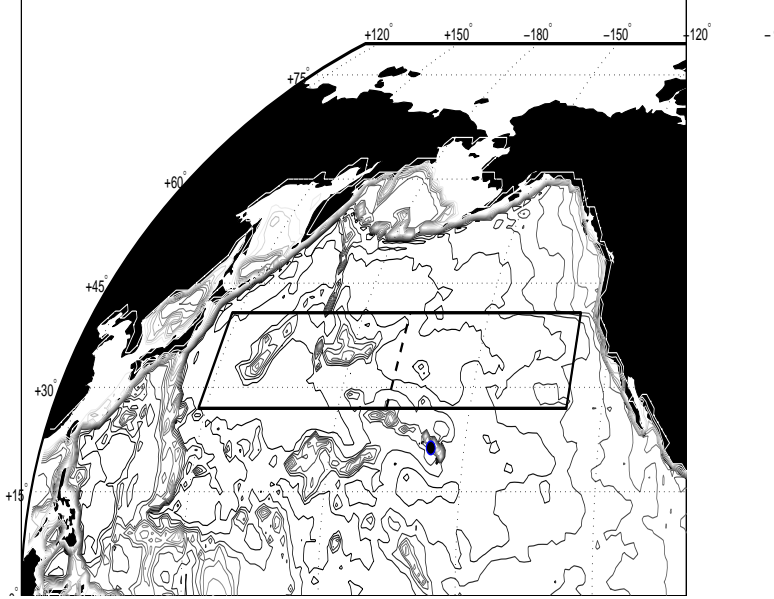


Figure 1: Region used to study sea level and transport variability. Only the eastern half of the box (east of dashed line) is used for some of the spectral calculations to avoid the very energetic Kuroshio and Kuroshio extension region, but meridional transports are computed over the entire width.

{globalpositio

59 forced, modes reviewed e.g., by Philander (1978). Motions not consistent with free modes can
 60 exist because they are externally forced, or because turbulent cascades generate them through
 61 nonlinear interactions. But at the present time, little observational data exists indicating their
 62 importance—other than the altimetric spectral densities—and these surface-trapped motions
 63 are ignored in what follows.)

64 Let $\eta(x, y, t)$ be the surface elevation at any lateral point x, y , and let $\Delta\eta(y, t)$ be the
 65 difference $\eta(x + L, y, t) - \eta(x, y, t)$. If the vertical structure of a geostrophic flow field, $V(z)$, is
 66 known, then the total transport of volume or mass above any depth z_1 , is readily computed as,

$$T(y, t) = \frac{g}{f} \frac{\Delta\eta(y, t)}{L} L \int_{z_1}^{\eta} V(z) dz = \frac{g}{f} \Delta\eta(y, t) \int_{z_1}^{\eta} V(z) dz \quad (1) \quad \{\text{transport1}\}$$

67 independent of L , as long as bottom topography does not intervene over the distance L . We
 68 now explore the consequences of this relationship, for illustration purposes, in the region shown
 69 in Fig. 1 and which occupies a large region of the subtropical gyre of the North Pacific Ocean.
 70 The western side is under the influence of the Kuroshio and its extension, while the eastern side
 71 might be regarded as typical of an oceanic interior. Pacific data are used here simply because
 72 they permit use of the largest distances and thus perhaps show the strongest spatial coherences.

73 Suppose now that the simplification is made that the water column structure $V(z) \propto F_1(z)$

74 where $F_1(z)$ is the first flat-bottomed baroclinic mode (Fig. 2), which has a zero crossing above
75 about 1400m (the shape is a slowly changing function of position). Consider the AVISO gridded
76 altimeter data (see Le Traon et al., 1998, for a discussion), at weekly intervals at the four corners
77 of the box shown in 1. The time series for the altimetric heights, are shown in Fig. 3 and Fig.
78 4 displays their power densities. The latter have a general red noise character, becoming nearly
79 white at periods longer than about 3 years. Records from the northern limit of the box show a
80 weak annual cycle as indicated in the figure.

81 Visually there is little resemblance among the time series. Of more immediate interest is the
82 coherence related to the meridional volume transport. Fig. 5 shows the coherence of $\Delta\eta$ over
83 the box width at meridional separations of $1^\circ, 3^\circ, 5^\circ, \dots$ of latitude relative to the box southern
84 boundary. With a latitudinal separation of 1 degree, there is a high coherence, although not
85 uniformly, down to periods as short as about 100 days. By three degrees of latitudinal separation,
86 there is no statistically significant coherence at 95% confidence until periods of almost three
87 years are reached. At five degrees of meridional separation, even 15 years of data produces no
88 apparent coherence and what coherence there is would account for a very small fraction of the
89 total variance.

90 These results are an extension to a much longer space scale of the results sketched by Wun-
91 sch (2008) who suggested that many decades would be required to obtain results indicative of
92 circulation trends in the large-scale ocean circulation. (H. Johnson and D. Marshall, personal
93 communication, 2009, have suggested that eddy noise might be substantially reduced as one
94 approaches the western boundary. Although that is possibly true for the North Atlantic near
95 25°N , the present results apply to the open ocean, and the increase of energy toward the west,
96 which is apparent in the power density spectra of Fig. 4, is consistent with expectations of the
97 most elementary physics.)

98 The incoherence seen in Fig. 5 is not a consequence of the presence of the Kuroshio. Fig.
99 6 shows the coherence estimate for a 12-degree meridional separation using only the data east
100 of the dashed line in Fig. 1. Thus even in the reduced eddy energy region, there is no useful
101 coherence at 12° latitudinal separation after 15 years. Whatever large-scale trends are present
102 in the circulation are invisible here.

103 **3 Frequency-Wavenumber Spectra**

104 The lack of large-scale coherence and the general dominance of the spectra by low frequencies
105 raises the question of the nature of the variability making up the altimetric records, and atten-
106 tion is now turned toward obtaining a partial understanding. One useful quantitative descriptor

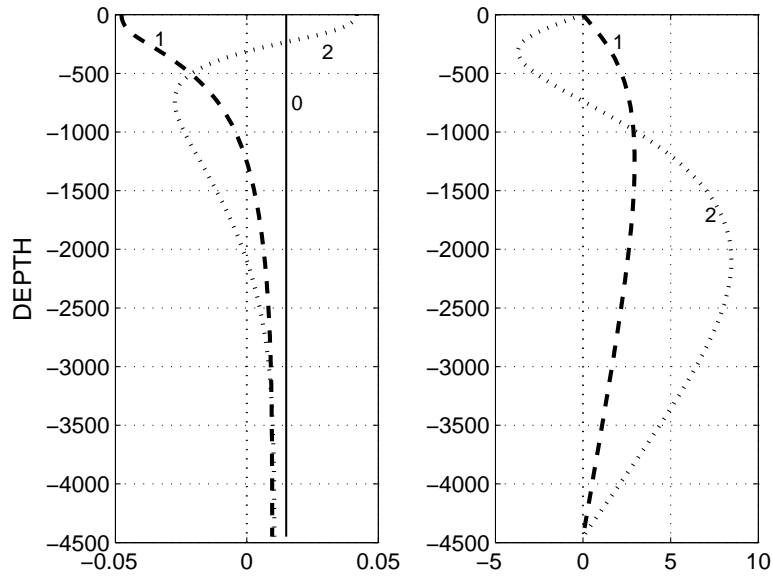


Figure 2: Shapes of the first 3-modes ($n = 0, \dots, 2$) at longitude $\lambda = 220^\circ\text{E}$ for horizontal velocity or pressure (left panel) and vertical displacement (right panel). Vertical displacements in the barotropic mode are linear with depth (increasing upwards), but much too small to be visible in the plot. Note that the surface boundary condition here precludes a buoyancy disturbance there—an issue of concern in a different context.

{mode_shapes.e

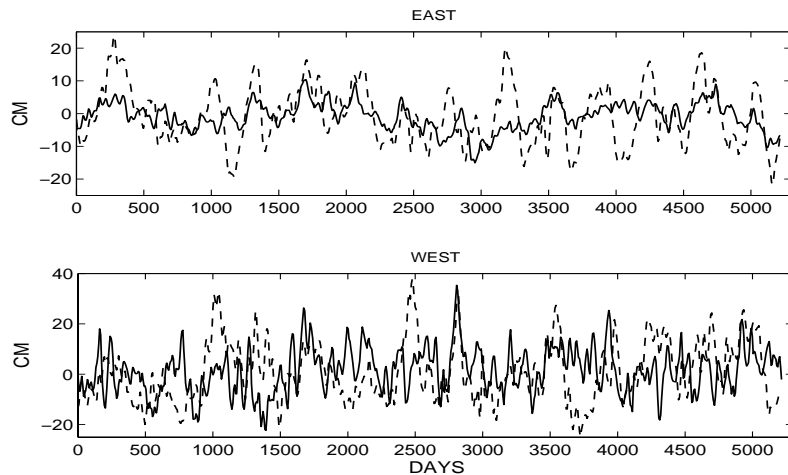


Figure 3: Upper panel is the altimetric height at the southeast (solid) and northeast (dashed) corners of the box, and lower panel shows them for the southwest (solid) and northwest (dashed) corners. That there is little visual coherence is apparent.

{east_west_ts.

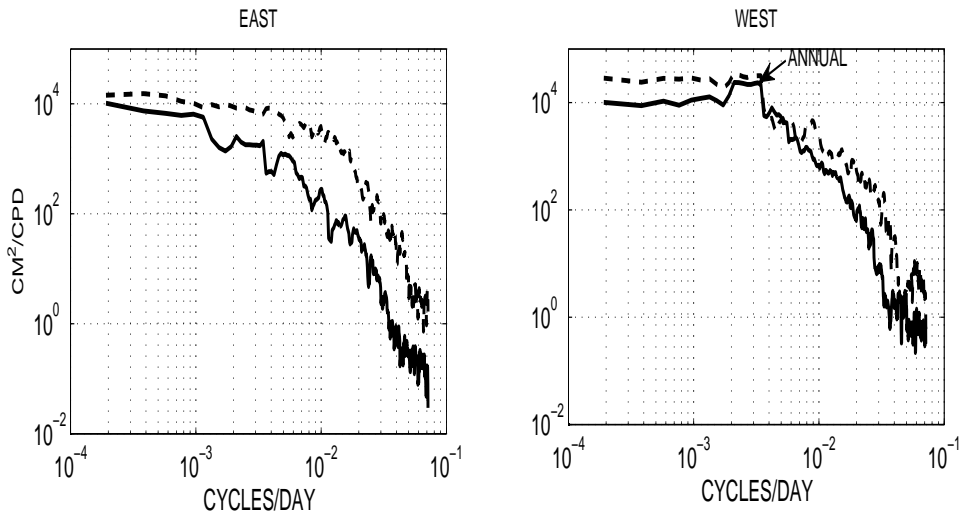


Figure 4: Multitaper spectral density estimates at the four corners of the analysis box. Because they are incoherent, the power density of the surface velocity between these two positions will be the sum of the spectra, and thus dominated by that at the western end. Multitaper spectral estimates are biased at the lowest frequencies and thus are slightly “redder” than is apparent here.

{pd_east_west_

107 of oceanic variability is its frequency/wavenumber spectrum. Such a description, although in-
 108 complete because of the strong spatial inhomogeneity, is an essential element in determining
 109 the significance of apparent trends and other low frequency variations, and its reproduction is a
 110 central test of skill in a general circulation model. Zang and Wunsch (2001, hereafter ZW2001)
 111 made an attempt to synthesize such a description from the data then available to them. A
 112 specific analogy to the original strawman internal wave model of Garrett and Munk (1972) was
 113 intended. The result assumed a restricted form of velocity component isotropy and did not
 114 represent the known anisotropic propagation of disturbances preferentially to the west. This
 115 supposedly universal form was spatially modulated by a complicated function of latitude and
 116 longitude independent of k, s . The present paper discusses some of the elements needed in future
 117 attempts at an improved synthesis.

118 Since the ZW2001 work, the high accuracy altimetric record has been extended from the four
 119 years available to them, to 15 years (at the time of writing) and this extended record opens the
 120 possibility of a more refined result. One element of the data—its representation of the altimetric
 121 data as showing “too-fast” Rossby waves (Chelton and Schlax, 1996)—received a remarkable
 122 degree of theoretical attention, notwithstanding its subsequent repudiation by Chelton et al.
 123 (2007). The latter authors concluded that there is no evidence for linear Rossby waves (D.

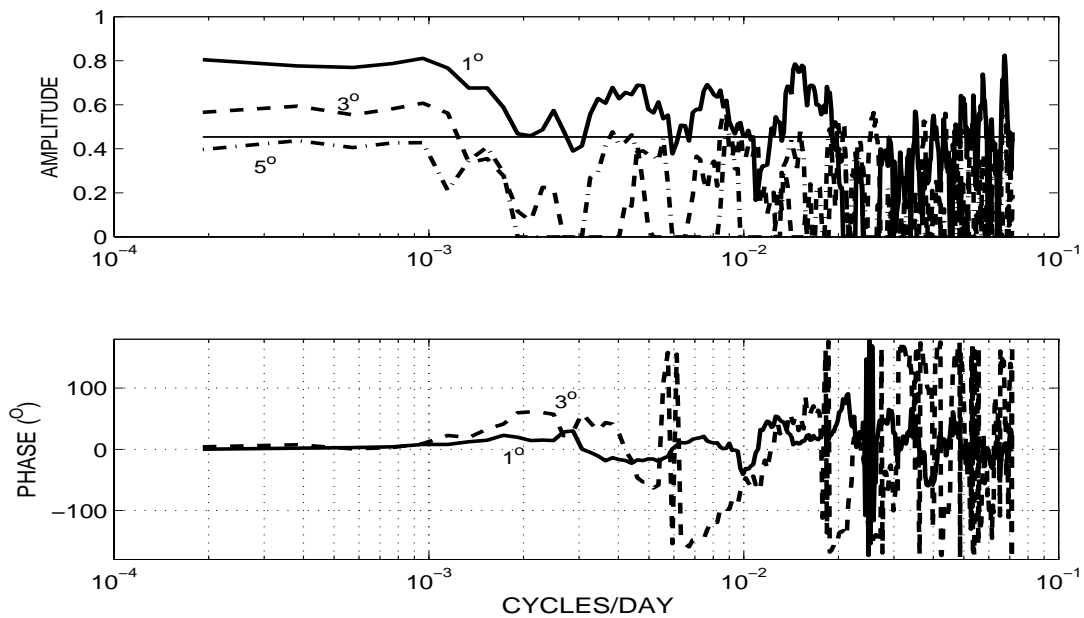


Figure 5: Coherence estimate of the apparent transport between the eastern and western sides of the box at separations of $1^\circ, 3^\circ, 5^\circ$ meridional separation. At 5° separation there is no apparent coherence even with 15 years of data and results for larger separations are not shown. (A multitaper coherence estimate. An approximate level-of-no-significance at 95% confidence is shown as the horizontal line.) Phases are not statistically meaningful when the amplitude is below the level-of-no-significance, and are thus not shown for separations beyond 3° latitude separation.

{trans_coher_n

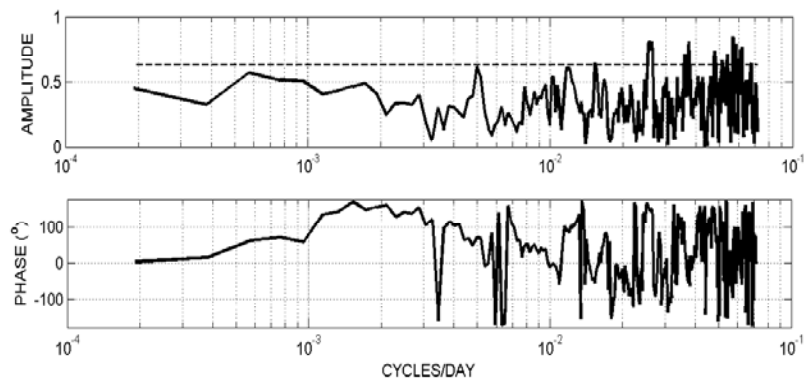


Figure 6: As in Fig. 5 except over 12 degrees meridional separation with the east-west separation taken from the center of the box to the eastern boundary. There is no significant coherence at any frequency at this separation.

{trans_coher_1

124 Chelton, private communication, 2009). Furthermore, the issue of the vertical structure, which
 125 was the focus of the mooring study of Wunsch (1997), has been put into context by theoretical
 126 and modeling studies (e.g., Smith and Vallis, 2001; Scott and Arbic, 2007; Ferrari and Wunsch,
 127 2009) of the existence of both up- and down-scale cascades in oceanic balanced motions. These
 128 discussions and debates have consequences for an improved representation of the frequency-
 129 wavenumber spectrum and ultimately its use in discussions of trend determination. Altimetric
 130 data now exceed in duration almost all oceanographic data sets and represent the only near-
 131 global dynamically relevant measurements that we have. Thus their understanding is in turn
 132 central to understanding of ocean circulation variability and the particular problem of trend
 133 determination. The present analysis is not comprehensive, but is intended to call attention to
 134 some of the issues in understanding the mid-latitude variability producing the incoherent results
 135 of the previous section.

136 Visual displays of the altimetric behavior in time and longitude (e.g., Fig. 7) show striking
 137 westward propagation of patterns and usually interpreted as Rossby waves. Chelton and Schlax
 138 (1996) interpreted the visual phase lines as linear, first baroclinic mode Rossby waves and showed
 139 that their apparent phase velocity tended to be higher than the theory predicted.

140 It is worth listing the major assumptions underlying what it is reasonable to call the “basic
 141 textbook theory” (BTT)¹ that was being compared to the observations. Those assumptions

¹The long history of Rossby waves is summarized by Platzman (1968).

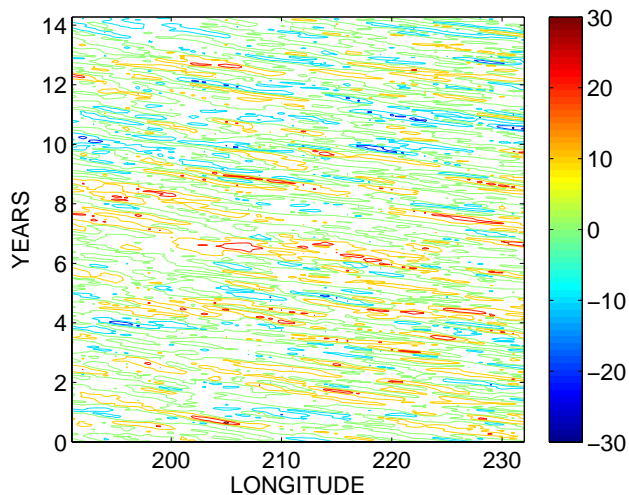


Figure 7: Longitude/time diagram for sea surface elevation, η , (cms) at latitude 29.25°N in the area in Fig. 1, confined to the east of the obvious Kuroshio extension. The westward phase propagation is visually dominant and important, but raises the question of how much of the variability is not described by these non-dispersive waves.

{long_time_dia

142 constitute a model of an ocean that:

- 143 (1) has a flat bottom
- 144 (2) has horizontally uniform stratification
- 145 (3) is otherwise at rest
- 146 (4) is represented by a tangent plane approximation to a sphere (the β -plane)
- 147 (5) is unforced
- 148 (6) has completely linear dynamics
- 149 (7) is laterally unbounded

150 This list is not complete (e.g., the Boussinesq approximation is also made). Of course, none
 151 of these assumptions is strictly correct and that the BTT works as well as it seems to is perhaps
 152 the real surprise.

153 Consider, as an example, the region shown in Fig. 1, the eastern side of the box used above
 154 to discuss the transport variability. The region is a representative one (to the extent that any
 155 ocean region can be so described), at least of the subtropical gyres. The data are again the
 156 gridded fields provided by AVISO and smoothed using the algorithm of Le Traon et al. (1998).
 157 Smoothing and gridding change the spectral content of a data set, but in the present case are
 158 not believed to introduce any significant distortion. Fig. 7 displays a time-longitude diagram
 159 for surface elevation, $\eta(x, y_c, t)$ along latitude 29.25°N in the box. The human eye evolved into

160 an extremely powerful instrument for pattern detection, and which one here sees very clearly as
161 the westward propagation in Fig. 7. The eye is not, however, very good at producing estimates
162 of the other motions present—motions that produce less marked patterns. Zang and Wunsch
163 (1999) using Fourier methods to separate different frequencies and wavenumbers, concluded that
164 at the longest wavelengths and lowest frequencies, with about 40% of the observed variance, the
165 motions had structures in frequency/wavenumber space indistinguishable from the BTT. As
166 the wavenumber and frequency magnitudes increased, significant deviations from the BTT were
167 plainly present—as Chelton and Schlax (1996) had pointed out. The results appeared to apply
168 at all low and mid-latitudes of the North Pacific that they examined.

169 A full quantitative oceanic description, however, attempts to break the motions down by
170 frequencies and wavenumbers, separates eastward/westward and northward/southward propa-
171 gation and distinguishes motions consistent with elementary theory from those requiring more
172 complicated explanation. (Chelton and Schlax (1996) and several others (e.g. Lecointre et al.,
173 2008—a model study) have used a so-called Radon transform to determine the dominant phase
174 velocity in these data. The Radon transform, perhaps best known in its tomographic appli-
175 cations (see Rowland, 1979), is computed by integrating the field along all straight pathways
176 defined along all angles in data fields such as in Fig. 7. One can then find those path angles
177 which maximize the integral and use them used to define the signal phase velocity. All fre-
178 quencies and wavenumbers contributing to the dominant phase velocity are lumped together.
179 Of equal interest, however, is knowledge of the fraction of the total energy accounted for by
180 that phase velocity band. Because the Radon transform can be converted into a Fourier trans-
181 form (e.g., Rowland, 1979) its information content is no more nor less than that of the Fourier
182 approach used here. The information content of the Fourier transform is complete—as is the
183 Radon transform if the integrals along *all* pathways are provided. Information by frequency and
184 wavenumber band has typically proved enlightening in wave propagation problems, even those
185 containing important nonlinearities.)

186 Another consideration worth keeping in mind is that *phase velocity* structures in observed
187 fields are commonly not fundamental physical properties of the motions. The best known dis-
188 cussion of the problem is probably that by A. Sommerfeld and L. Brillouin who showed that
189 electromagnetic phase velocities exceeding the speed of light were not a contradiction to special
190 relativity. Rather it was the group velocity, which has physical meaning as the rate and direction
191 with which energy and information flow, that remained fundamental (see Brillouin, 1960, for an
192 extended discussion). In a general context, phase lines are kinematic interference patterns and
193 so subject to distortion by a wide variety of phenomena including boundary positions. So for
194 example, Frankignoul et al. (1997) point out that introducing an eastern wall in the presence of

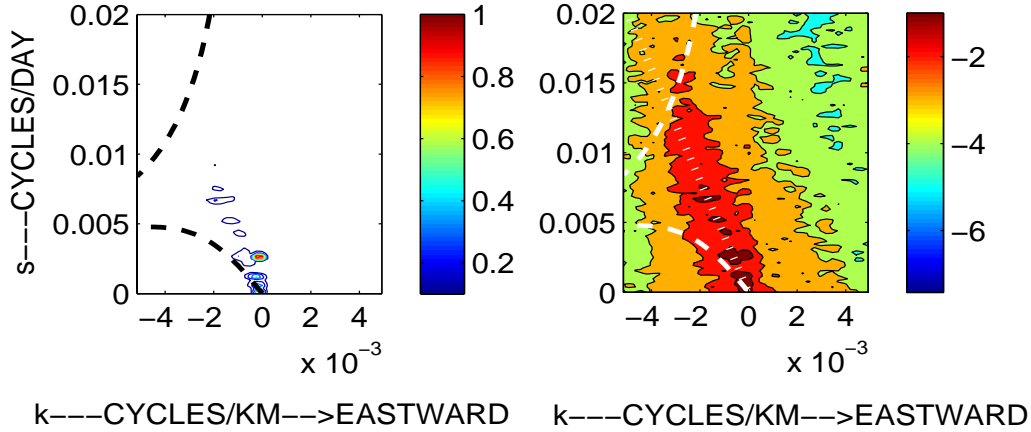


Figure 8: Frequency (cycles/day) and zonal wavenumber (cycles/km) along the southern edge of the box. Left panel is from the two-dimensional periodogram plotted on a linear power scale, smoothed in frequency and wavenumber so as to be χ^2 variables with about 8 degrees of freedom in each estimate (averaged over two frequencies and two wavenumbers). Right panel displays the logarithm of the power. Dashed curves indicate the first baroclinic mode, $l = 0$, basic dispersion curve. The “non-dispersive line” defined in the text lies along the ridge of maximum energy density and closely approximated by the dotted white line (slope is 4km/day).

{region1_east_

195 BTT Rossby waves immediately produces naively-determined zonal phase velocities that are a
 196 factor of two larger than the BTT dispersion relationship. A full Fourier procedure, as we use,
 197 that accounts for standing wave components would not display such a discrepancy.

198 Figure 8 shows the estimated frequency-wavenumber spectra, $\Phi(k, s)$ for a fixed latitude
 199 (27° – –the southern edge of the area) from a mildly smoothed (over two frequency and two
 200 wavenumber bands). The dispersion curves are shown for the barotropic, and lowest vertical
 201 baroclinic mode with $l = 0$, and a first mode having a deformation radius, $R_d = 35\text{km}$. Consis-
 202 tent with the result of Zang and Wunsch (1999, their Figs. 4, 5), at the very lowest observable
 203 frequencies and wavenumbers, the energy maximum is indistinguishable from the dispersion
 204 curve. With increasing frequency (and corresponding wavenumber), deviations from the curve
 205 are seen, as pointed out by Chelton and Schlax (1998). Consistency with the dispersion curve
 206 of the BTT does not prove that those low frequency motions are BTT Rossby waves, but does
 207 remove the main evidence that they are incompatible with it. For larger magnitude frequencies
 208 and wavenumbers, the deviation is quite marked, with higher apparent phase and group veloc-

ities and phase velocities tending toward the much higher values predicted for the barotropic mode.

The energy maximum lying approximately along the straight line $\gamma k + s = 0$, $\gamma \approx 4\text{km/d}$ is quite striking and as it implies non-dispersive motions, we will call it the “non-dispersive line”. It reaches all the way from the lowest estimated frequency to the barotropic dispersion curve. As in Zang and Wunsch (1999), γ is approximately the long-wavelength (non-dispersive limit) group velocity of the first baroclinic mode. They found it to be universally present in all the areas they analyzed. No theory has so far explained this striking characteristic of oceanic variability. Note, however, that the peak at the annual cycle is indistinguishable from $k = 0$. Whether the non-dispersive line is truly tangent to the baroclinic dispersion curve as $s \rightarrow 0$ is not clear and as the period approaches infinity, many physical complications can ensue. From the results of Longuet-Higgins (1964), one might have anticipated an energy maximum where the zonal group velocity of the first baroclinic mode vanishes, where $\partial s / \partial k = 0$ (in analogy to the arguments of Wunsch and Gill, 1976, for the equatorially trapped gravity modes), but there is no obvious evidence for such a structure here.

It is, of course, possible that a much stronger effective β , arising from the background potential vorticity gradient (e.g., Killworth et al., 1997), would push the non-dispersive, low wavenumber end of the first baroclinic mode dispersion curve to much higher values. That the non-dispersive line touches the barotropic dispersion curve—implies a very large increase in effective β , and the general evidence, taken up below, of vertical structures involving strongly coupled barotropic and baroclinic modes. Note that the zonal mean surface velocity over the entire area is about 0.05cm/s and its RMS is about 0.2cm/s and so unlikely to cause first-order distortions in the dispersion relation. (It is important to recall, however, that the gridded altimetric data are smoothed, and thus will tend to underestimate the RMS velocity field. Time means are also subject to errors in the estimated geoid.)

Some measure of the relative importance of the energy lying along the non-dispersive line is obtained by finding the cumulative sum over k , for each frequency, s , and normalizing it by the total:

$$C(k, s) = \frac{\int_{-k_{\max}}^k \Phi(k, s) ds}{\int_{-k_{\max}}^{k_{\max}} \Phi(k, s) ds}$$

and which is plotted in Fig. 13 as a function of k for various values of s . At low frequencies, where the motions are indistinguishable from BTT Rossby waves, the non-dispersive line is the major fraction of the energy; at high frequencies, it has disappeared altogether as a noticeable feature. Thus at periods shorter than about 100 days, the unstructured spectral model of ZW2001 is reasonably accurate, but it fails to account for the excess non-dispersive motions at

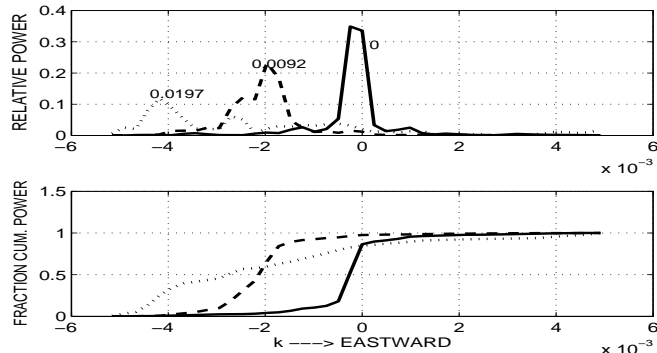


Figure 9: Upper panel shows the values for three values of s in cycles/day of the smoothed estimated power spectral density displayed in Fig. 8 and the lower panel shows the accumulating sum. Frequency separation is logarithmic between $s = 0$ and $s = 0.2$. The energy excess on the non-dispersive line is seen as a large near-jump in the integrated values. At the lowest frequencies, the neighborhood of the non-dispersive line contains about 80% of the energy, falling to an undetectable excess about the background at the highest frequencies (the accumulating sum is there nearly linear). All values were normalized so that the sum of the power over k at fixed s is unity. Most of the low frequency energy is westward going, becoming more nearly equipartitioned at the highest frequencies.

{pd_frac_summe

242 low frequencies.

If the frequencies and wavenumbers are summed out, one obtains the zonal wavenumber, $\Phi_k(k)$, and frequency, $\Phi_s(s)$. That is,

$$\int_0^{\infty} \Phi(k, s) ds = \Phi_k(k), \quad (2) \quad \{\text{analyt1}\}$$

$$\int_{-\infty}^{\infty} \Phi(k, s) dk = \Phi_s(s). \quad (3) \quad \{\text{analyt2}\}$$

243 shown in Fig. 10. Φ_k shows the strong k^{-4} roll-off noted by Stammer (1997) on spatial scales
 244 shorter than about 500km. (ZW2001 used $k^{-5/2}$ above 1/400km.) In this particular region, the
 245 eastward-going variance is about 29% of the total, and its wavenumber spectrum has a different,
 246 near power-law, rednoise behavior. Because Stammer (1997) used along-track data, the rapid
 247 roll-of is not a consequence of the mapping (smoothing) methodology employed at AVISO.
 248 The frequency spectrum here falls at a rate closer to s^{-3} than the s^{-2} value used by ZW2001
 249 which, however, included the more energetic western part of the ocean. At low frequencies, a fit
 250 excluding the annual peak gives a power law close to $s^{-0.3}$, roughly consistent with ZW2001.

251 Fig. 11 is a time-*latitude* diagram. Visually, the pattern is much more like a standing wave,
 252 although the amplitude modulation with latitude shows that wavenumbers other than $l = 0$
 253 must be involved and they must be phase-locked. In the discussion of dispersion relations for

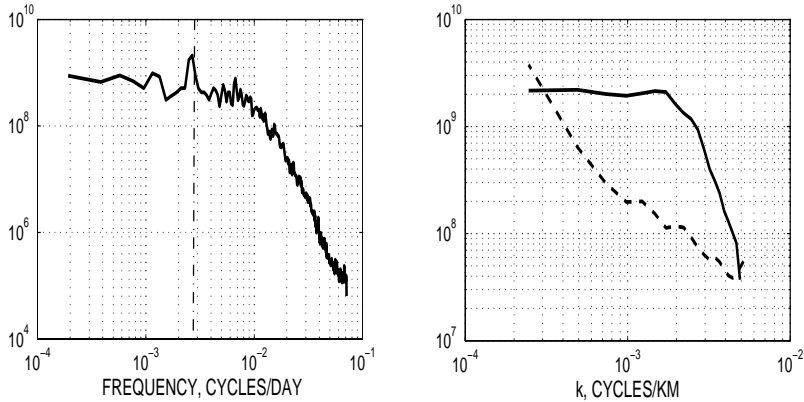


Figure 10: Frequency, $\Phi_s(s)$ (left panel), and zonal wavenumber, $\Phi_k(k)$, spectra of η for the eastern part of the study region. Wavenumber spectra are shown as westward-(solid) and eastward- (dashed) going energy. Dash-dot line denotes the annual cycle which is only a small fraction of the total energy and which (see Fig. 8) is dominated by the lowest wavenumbers, indistinguishable here from $k = 0$.

Approximate 95% confidence limits can be estimated as the the degree of high frequency or wavenumber variability about a smooth curve and are quite small.

{one_dspectra.

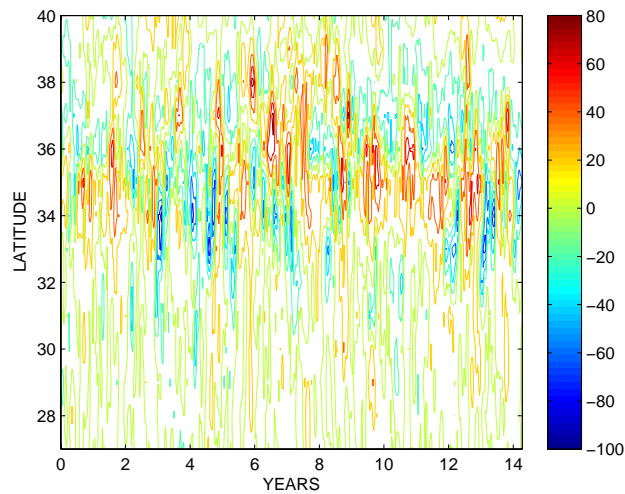


Figure 11: A time-latitude diagram of sea surface height in cms along a meridional line (211°E) across the box in Fig. 1. Visually, the motions are close to standing oscillations in time, and for simplicity are so regarded here, although the latitudinal wavenumbers are finite.

{lat_time_diag

spectrum.tif

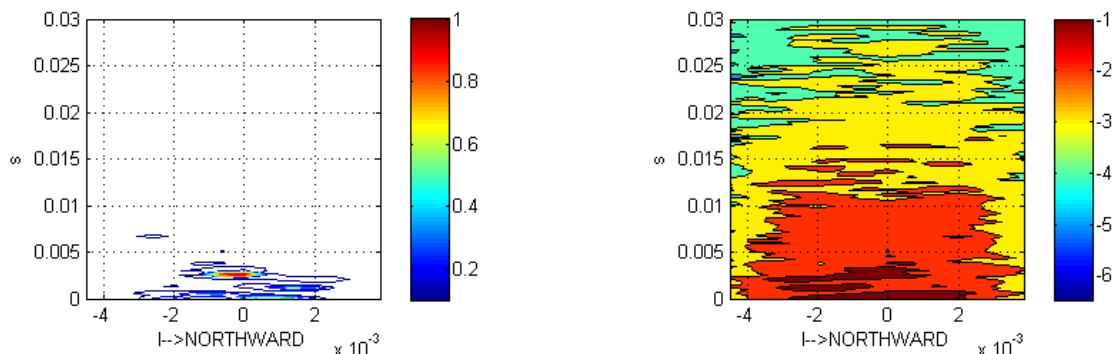


Figure 12: Frequency-wavenumber (in l) spectra corresponding to Fig. 8. Somewhat more energy propagates northward than southward.

{region1_east_

254 the zonal motions, $l = 0$ as was assumed for simplicity. Fig. 12 shows the linear and logarithmic
 255 contours of (l, s) power density from the 15° latitude band across the box. While the energy
 256 is clearly clustered around $l = 0$, significant amounts are found at finite values. Fig. 8 shows
 257 that there is finite energy at scales shorter than 1000km, but longer than the Rossby radii, that
 258 ultimately must be taken into account (postponed). In terms of the BTT dispersion relationship,
 259 finite l pushes all the baroclinic modes to yet lower frequencies, and thus has little effect on the
 260 structure near $s = 0$, where much of the energy is nearly tangent to the $n = 1$ curve. Note the
 261 slightly reddish nature of the low frequency spectrum.

262 4 Vertical Structure

263 The discussion of transports as inferred from altimetry is directly dependent upon the vertical
 264 structure underlying the surface motions. In the schematic of Wunsch (2008), it was assumed
 265 that all of the motions lay in the first baroclinic mode. A rough rule of thumb is that about
 266 50% of the mesoscale kinetic energy is in the barotropic mode (with “barotropic” specifically
 267 defined above) with about 40% in the first baroclinic one (Wunsch, 1997).² This inference is
 268 based upon the current meter data available at that time and was used by ZW2001 as part
 269 of their spectral description. There was considerable evidence of “phase-locking” of the modes

²That roughly half the kinetic energy at periods shorter than about a year is best described as “barotropic” has often been simply ignored in theories focussing on the first baroclinic mode.

270 in some regions, albeit the coverage was inadequate to generalize about it. Such phase-locking
 271 can be an indication of non-linearity in the system, consistent e.g. with McWilliams and Flierl
 272 (1976) and the inference of Chelton et al. (2007) that a linear Rossby wave description is at best
 273 incomplete—as one infers from Fig. 2. Apparent phase locking can also occur from the linear
 274 interaction of any particular vertical mode with topographic gradients—which necessarily then
 275 couple all the modes. Klein et al. (2008) discuss the plausible existence of trapped near-surface
 276 motions, dependent upon near-surface shear. There is no immediate evidence that such motions
 277 are visible in the altimetry on the space/time scales now accessible. In any event, vertical
 278 modes are a complete set, although possibly an inefficient one near $z = 0$ if surface buoyancy
 279 distributions are important. If the modes are coupled, as they appear to be, a full description
 280 requires specification of their phase, in addition to their mean-square amplitude as a function
 281 of frequency.

282 With very rare exceptions, current meter records have a duration of less than a year and the
 283 set of water-column spanning current meter or temperature moorings of long duration is almost
 284 empty. The question then arises as to the vertical partition of oceanic kinetic energy on the time
 285 scales exceeding that of geostrophic eddies (longer than about one year) and on spatial scales
 286 greater than a few hundred kilometers. A useful estimate is particularly important in the design
 287 of in situ arrays for trend determination in the general circulation. Using the global hydrography,
 288 Forget and Wunsch (2007) showed that vertical displacements could be interpreted in most
 289 regions as owing primarily, but not completely, to the first baroclinic mode. Hydrographic data
 290 used that way does not, however, permit any inferences about barotropic motions.

291 That the dominant observed motions are a combination of barotropic and baroclinic mode-
 292 like structures embedded in a broadband (in frequency and wavenumber) background of more
 293 linear motions is an inference consistent with the frequency/wavenumber content in Fig. 8, the
 294 “too fast” phase velocity of Chelton and Schlax (1996), the coherent vortex picture of Chelton
 295 et al. (2007), and the coupled mode picture from current meter moorings of Wunsch (1997).
 296 The amount of information available about the details of the coherent vortex structures, which
 297 we tentatively identify with the non-dispersive line, is, however, minimal. We therefore propose
 298 as a strawman hypothesis that the energy density for the motions is proportional to the relative
 299 distances to the barotropic and first baroclinic mode dispersion curves with $l = 0$,

$$s = -\frac{\beta k}{k^2 + 1/R_i^2}, \quad i = 0, 1, \quad R_1 = 35\text{km}. \quad (4) \quad \{\text{dispersion1}\}$$

300 For numerical purposes, R_0 was set to infinity so as to avoid the presence of the long-wave
 301 branch of the barotropic mode, which otherwise leads to a complicated multivaluedness in the
 302 distance to the dispersion curve. Define r_0, r_1 as the minimum distance from any location, k^*, s^*

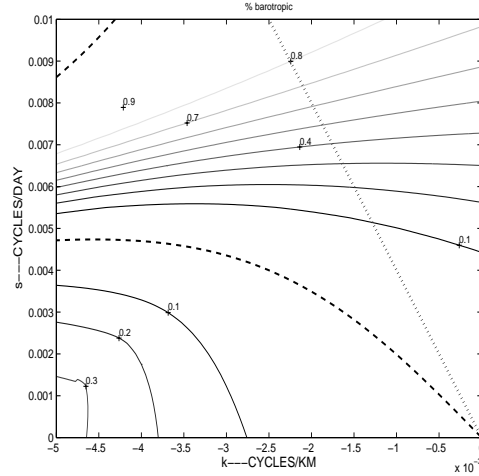


Figure 13: Fraction of the variance hypothesized to lie in the barotropic mode and based upon the distance in k, s space from the two BTT dispersion curves (dashed lines). Westward-going motions only. Dotted line is the non-dispersive line with an energy maximum, and for which at low frequencies the motion would be almost completely baroclinic. At the present time, there is no information concerning the vertical structures for frequencies and wavenumbers lying below the $n = 1$ dispersion curve nor those above that for $n = 0$.

{mode_distance

303 to the two dispersion curves, Eq. (4). Then their values are found numerically and plotted in
 304 Fig. 13.

305 A conjecture, based on only the fragmentary evidence already cited, is that we can partition
 306 the energy in the vertical as,

$$\frac{1}{r_1^2 + r_0^2} \left[r_1^2 (1 - r_0^2) F_0^2(z) + r_0^2 (1 - r_1^2) F_1^2(z) \right]$$

307 (not allowing for phase coupling), that is, depending upon the relative distances to the two
 308 dispersion curves. One could evidently extend such a rule to incorporate the distances to the
 309 dispersion curves of the higher baroclinic modes, but as we are essentially without any supporting
 310 information, that step is omitted here. Wunsch (1997) used the ratio of the surface kinetic energy
 311 computed directly from u, v to that computed from the sum of squares of the esimated modal
 312 amplitudes at the surface. Uncoupled modes should produce a ratio of one and wide variations,
 313 both above and below one were found, but no simple spatial pattern could be discerned. Most
 314 mooring records are too short to produce definitive results on modal coupling. Whatever the
 315 partition, it is important to note that many other structures are also present in the data.

316 5 Summary Comments

317 At the present time, the longest accessible periods are about 15 years, and the question of the
318 nature of much lower frequency oceanic variability is open, and requires separate study. Although
319 eddy-resolving regional general circulation models now exist, little or no data are available to
320 test their conclusions. (The constrained state estimate with 1° horizontal resolution discussed by
321 Wunsch and Heimbach, 2008, shows a reduced, but non-zero, barotropic contribution at periods
322 exceeding a year. No information is readily available to test that result and it is not further
323 discussed.) To the extent that the altimetry of the particular subtropical region, supplemented
324 by some mooring and other data, are typical of the global ocean, a few simple summary elements
325 concerning the shorter periods, can be described:

326 Oceanic variability at these latitudes exhibits a broad-band character in both frequency and
327 wavenumber including significant eastward motions. Theory would suggest that much of this
328 motion is forced meteorologically and/or is the result of turbulent cascades, but this inference
329 has not been explored. At low frequencies and wavenumbers the motions are, from the proximity
330 to the BTT dispersion curve, indistinguishable in altimetric data alone from linear Rossby waves.

331 In the band of frequencies from about 1 cycle/15 years to about 1 cycle/4 months, sur-
332 face pressure variability (surface elevation) exhibits an excess of energy along the nearly non-
333 dispersive line lying between the first baroclinic and barotropic modes. These motions are
334 inferred to represent a non-linear coupling of these modes. It is *conjectured* that the relative
335 fraction of the energy in the modes is inversely proportional to their distance in wavenumber-
336 frequency space to the BTT dispersion curves, and that the coherent eddies discussed by Chelton
337 et al. (2007) are best described this way.

338 The origins of the non-dispersive motions have not been discussed. Coherent vortex dy-
339 namics, or Korteweg-DeVries types of soliton motions could be investigated. and some kind of
340 wave-turbulence interaction could conceivably give rise to such behavior. It does seem to be a
341 robust feature of the altimetric data.

342 Much more remains to be done, including making the analysis global (C. Hughes, personal
343 communication, 2009) and in particular a special discussion of the Southern Ocean is needed—
344 as it tends to be different in most ways. Better understanding of the meridional structure of
345 the motions, theoretical understanding of the non-dispersive line, and of the vertical partition
346 of the energy are all needed. Alternative and perhaps more quantitatively accurate analytic
347 frequency-wavenumber descriptions would be useful. How increasingly complex eddy-resolving
348 general circulation models are to be tested is not obvious.

349 *Acknowledgements.*

350 I had useful comments from G. Flierl, R. Ferrari, P. O’Gorman, P. Cummins, D. Gilbert
351 and two anonymous reviewers. Supported in part by the Jet Propulsion Laboratory (NASA)
352 through the Jason-1 program, the National Ocean Partnership Program (NASA and NOAA). I
353 thank Chris Garrett for providing the necessary excuse for a nice party, and for many years of
354 provocative interaction.

355

356

References

- 357 Brillouin, L., 1960: *Wave Propagation and Group Velocity*. Academic, New York, 154p.
- 358 Chelton, D. and M. G. Schlax, 1996: Global observations of oceanic Rossby waves. *Science*,
359 272, 234-238.
- 360 Chelton, D. B., M. G. Schlax, R. M. Samelson, R. A. de Szoeke, 2007: Global observations
361 of large oceanic eddies. *Geophys. Res. Letts.*, 34(15), L15606.
- 362 Ferrari, R.; Wunsch, C., 2009: Ocean circulation kinetic energy: Reservoirs, sources, and
363 sinks. *Ann. Rev. Fl. Mech.*, 41, 253-282.
- 364 Forget, G.; Wunsch, C., 2007: Estimated global hydrographic variability. *J. Phys. Oc.*, 37,
365 1997-2008.
- 366 Frankignoul, C., P. Müller and E. Zorita, 1997: A simple model of the decadal response of
367 the ocean to stochastic wind forcing. *J. Phys. Oc.*, 27, 1533-1546.
- 368 Garrett, C. J. R. and W. H. Munk, 1972: Space-time scales of internal waves. *Geophys. Fl.*
369 *Dyn.*, 3, 225-264.
- 370 IPCC. Intergovernmental Panel on Climate Change, 2007: *Climate Change 2007 - The*
371 *Physical Science Basis*. Cambridge Un. Press, Cambridge, 1009pp.
- 372 Killworth, P. D., D. B. Chelton and R. A. de Szoeke, 1997: The speed of observed and
373 theoretical long extratropical planetary waves *J. Phys. Oc.*, 27, 1946-1966.
- 374 Klein, P., B. L. Hua, G. Lapeyre, X. Capet, S. Le Gentil, H. Sasaki, 2008: Upper-ocean
375 turbulence from high-resolution 3D simulations. *J. Phys. Oc.*, 38, 1748-1763.
- 376 Lecointre, A., T. Penduff, P. Cipollini, R. Tailleux, B. Barnier, 2008: Depth dependence of
377 westward-propagating North Atlantic features diagnosed from altimetry and a numerical 1/6
378 degrees model. *Ocean Science*, 4, 99-113.
- 379 Le Traon, P. Y., F. Nadal, N. Ducet, 1998: An improved mapping method of multisatellite
380 altimeter data. *J. Atm. Oc. Tech.*, 15, 522-534.
- 381 Longuet-Higgins, M. S., 1964: Planetary waves on a rotating sphere. *Proc. Roy. Soc. A*,
382 279, 446-473.
- 383 McWilliams, J. C. and G. R. Flierl, 1976: Optimal, quasi-geostrophic wave analysis of MODE
384 array data. *Deep-Sea Res.*, 23, 285-300.
- 385 Peacock, S. and M. Maltrud, 2006: Transit-time distributions in a global ocean model. *J.*
386 *Phys. Oc.*, 36, 474-495.
- 387 Percival, D. B., J. E. Overland and H. O. Mofjeld, 2001: Interpretation of North Pacific
388 variability as a short- and long-memory process. *J. of Climate*, 14, 4545-4559.

389 Philander, S. G. H., 1978: Forced oceanic waves, *Revs. Geophys.*, 16, 15-46.

390 Platzman, G., 1968: The Rossby wave, *Quat. J. Roy. Met. Soc.*, 94, 225-248.

391 Rowland, S. W., 1979: Computer implementation of image reconstruction formulas. in,
392 *Image Reconstruction from Projections. Implementation and Applications*, Herman, G. T., ed,
393 Springer-Verlag, Berlin, 9-80.

394 Schiermeier, Q., 2004: Gulf Stream probed for early warnings of system failure. *Nature*, 427,
395 769.

396 Scott, R. B.; Arbic, B. K., 2007: Spectral energy fluxes in geostrophic turbulence: Implica-
397 tions for ocean energetics. *J. Phys. Oc.*, 37, 673-688.

398 Smith, K. S.; Vallis, G. K., 2001: The scales and equilibration of midocean eddies: Freely
399 evolving flow, *J. Phys. Oc.*, 31, 554-571.

400 Stammer, D., 1997: Global characteristics of ocean variability estimated from regional
401 TOPEX/POSEIDON altimeter measurements. *J. Phys. Oc.*, 27, 1743-1769.

402 Wunsch, C., 1997: The vertical partition of oceanic horizontal kinetic energy. *J. Phys. Oc.*,
403 27, 1770-1794.

404 Wunsch, C. and A. E. Gill, 1976: Observations of equatorially trapped waves in Pacific sea
405 level variations. *Deep-Sea Res.*, 23, 371-390

406 Wunsch, C., and P. Heimbach, 2006: Decadal changes in the North Atlantic meridional
407 overturning and heat flux. *J. Phys. Oc.*, 36, 2012-2024.

408 Wunsch, C. and P. Heimbach, 2008: How long to oceanic tracer and proxy equilibrium?
409 *Quat. Sci. Revs.*, 27, 637-65.

410 Wunsch, C. and P. Heimbach, 2009: The global zonally integrated ocean circulation (MOC),
411 1992-2006: Seasonal and decadal variability, *J. Phys Oc.*, 39, 351-368.

412 Wunsch, C., R. Ponte, P. Heimbach, 2007: Decadal trends in global sealevel patterns, *J.*
413 *Climate*, 20, 5889-5911.

414 Zang, X. and C. Wunsch, 1999: The observed dispersion relation for North Pacific Rossby
415 wave motions, *J. Phys. Oc.*, 29, 2183-2190.

416 Zang, X. and C. Wunsch, 2001: Spectral description of low frequency oceanic variability. *J.*
417 *Phys. Oc.*, 31, 3073-3095.